A structural approach for 3D building reconstruction

Florent Lafarge, Xavier Descombes, Josiane Zerubia, Marc Pierrot-Deseilligny

INSTITUT NATIONAL DE RECHERCHE EN INFORMATIQUE ET EN AUTOMATIQUE

A structural approach for 3D building reconstruction

Florent Lafarge — Xavier Descombes — Josiane Zerubia — Marc Pierrot-Deseilligny

N°6048

November 2006

Thème COG

ISSN 0249-6399 ISRN INRIA/RR--9999--FR+ENG

A structural approach for 3D building reconstruction

Florent Lafarge * † , Xavier Descombes* , Josiane Zerubia * , Marc Pierrot-Deseilligny†

Thème COG — Systèmes cognitifs
Projets Ariana

Rapport de recherche n° 9999 — November 2006 — 37 pages

Abstract: In this report, we present a 3D building reconstruction method based on a structural approach. It consists in reconstructing buildings by assembling simple urban structures extracted from a grammar of 3D parametric models. This method is composed of two stages. The first one, which has already been tackled in previous works, consists in extracting the building footprints through configurations of connected quadrilaterals. The second stage, detailed in this report, corresponds to the 3D reconstruction from DEMs and obtained building footprints. An energy formulation is used within a Bayesian framework which is particularly well adapted to introduce prior knowledge related to urban structures and their assembling. In order to find the optimal solution of this energy, two different optimization techniques are used and compared.

Key-words: 3D reconstruction, building, urban area, structural approach, RJMCMC, Viterbi algorithm, marked point processes

* Projet Ariana - INRIA/I3S - Sophia-Antipolis - email=Name.Lastname@inria.fr
† Institut Géographique National - Saint-Mandé - email=Name.Lastname@ign.fr

Unité de recherche INRIA Sophia Antipolis
2004, route des Lucioles, BP 93, 06902 Sophia Antipolis Cedex (France)
Téléphone : +33 4 92 38 77 77 — Télécopie : +33 4 92 38 77 65

Une approche structurelle pour la reconstruction 3D de bâtiments

Résumé : Dans ce rapport, nous présentons une méthode de reconstruction 3D de bâtiments fondée sur une approche structurelle. Cela consiste à reconstruire des bâtiments en assemblant des structures urbaines simples, extraites d'une grammaire de modèles paramétriques 3D. Cette méthode est composée de deux étapes. La première, qui a déjà été abordée dans des travaux antérieurs, a pour but d'extraire les emprises de bâtiments sous forme de configurations de quadrilatères connectés entre eux. La seconde étape, détaillée dans ce rapport, consiste à reconstruire en 3D les bâtiments à partir de MNE et des emprises obtenues.Une énergie est définie dans un cadre bayésien, particulièrement intéressant pour introduire des connaissances a priori sur les structures urbaines et leurs assemblages. Afin de trouver la solution optimale de cette énergie, deux techniques différentes d'optimisation seront utilisées et comparées.

Mots-clés : reconstruction en 3D, bâtiment, zone urbaine, approche structurelle, RJMCMC, algorithme de Viterbi, processus ponctuels marqués

Contents

Notations

S	a set of sites s
I	a set of intensities Λ_s associated with S : $I = \{\Lambda_s / s \in S\}$
$\mathcal{Q}$	object space of a quadrilateral with marked edges
$\mathcal{C}$	quadrilateral configuration representing the building footprints of I ($\in \mathcal{Q}^N$)
N	number of quadrilaterals in $\mathcal{C}$
S_i	subset of S whose sites are inside the quadrilateral $i \in \mathcal{C}$
$\mathcal{D}$	the set of data defined by $\mathcal{D} = \{\Lambda_s \in I / s \in S_i \, , i \in \mathcal{C}\}$
$\mathcal{M}$	grammar of 3D-models
$\mathcal{T}$	state space
x	an element of $\mathcal{T}$ which corresponds to a configuration of 3D-parametric objects x_i knowing the quadrilateral footprints $\mathcal{C}$: $x = (x_i)_{i \in \mathcal{C}}$
$\mathcal{S}_{x_i}$	function from S_i to $\mathbb{R}$ which associates the roof height at each site of S_i
$\bowtie$	neighborhood relationship defined on $\mathcal{C}$
$h(.)$	posterior density on $\mathcal{T}$
$(X_t)_{t \in \mathbb{N}}$	Markov chain on $\mathcal{T}$
$\pi(.)$	target distribution defined on $\mathcal{T}$
T_t	sequence of temperatures
J	jump matrix
$\mathbb{1}_{\{A\}}$	the characteristic function which returns 1 if the condition A is true and 0 otherwise.

1 Introduction

The 3D building reconstruction is a difficult problem, mainly due to the complexity and the variability of the scenes. Urban environments are very dense and composed of many types of buildings. Therefore, their analysis remains an open problem in an automatic context.

1.1 State of the art

Many methods have been developed to extract and reconstruct 3D buildings in various contexts which depend on the automaticity and the kind of data. Hereafter we mention a few of them:

- Semi-automatic methods
  [3][9] propose semi-automatic processes which need human operator interventions. However, the 3D building reconstruction demands automaticity which is the case of the methods mentioned below.

- Single view image
  The input can be a single view image such as in [18]. Building shadows are used to extract 3D information. However using a single view does not allow to have a detailed reconstruction.

- Multiple view images
  Multiple view aerial images are the most common input. Such data are rich in terms of 3D information and allow to extract 3D primitives. For example, [14][28] use 3D lines in their reconstruction methods. In [13], planes are extracted and then arranged in a polyhedral approach. [1][29] propose generic models by combining several kinds of primitives. [7] uses a parametric approach based on marked point processes.

- Laser scanning
  Laser scanning is also very popular since the decrease of the acquisition cost and the accuracy of the measures. Some interesting models have been proposed using laser data such as [5][10][19].

- Digital Elevation Model (DEM)
  Several methods, such as [32][34], are based on DEMs. The use of DEMs is motivated by the fact that they already provide a geometric description of the scene from aerial imagery or airborne scanner data.

Nowadays, this problem can be tackled by another type of data: the sub-metric satellite images. The future PLEIADES satellites are especially well adapted to deal with 3D building reconstruction through the high resolution of images (0.7 meter) and the stereoscopic characteristics (three views - B/H=0.2). The main advantages of satellite data compared to aerial images are a high swath width and ground coverage. However, such data have a "relatively low" resolution and a "low" Signal to Noise Ratio (SNR) to deal with 3D reconstruction problems compared to aerial data. For example, PLEIADES simulations have 2 pixels per square meter density contrary to aerial images used in [6][29] which have about 25 pixels per square meter. In this report, we aim at automatically reconstructing buildings by exploiting satellite images, and more precisely PLEIADES simulations.

1.2 Global strategy

There are two main families of approaches in 3D building reconstruction. The first one corresponds to **generic modelings**. These kinds of approaches are theoretically able to reconstruct any shape of building through connected planar facets. However, they demand high resolution data and important computing times as mentioned in [1][13][28] or [29]. The second one is the **parametric modelings**. Although these reconstructions are limited (most of parametric models consider a symmetric two-plan roof reconstruction based on skeleton processes), they are known to be robust with respect to the data, see [3][7][19] or [34] for more details.

1.2.1 The structural approach

In this report, we propose an approach which is halfway between generic and parametric modelings : the **structural approach**. It consists in reconstructing buildings by merging simple urban structures extracted from a grammar of 3D parametric models (see Figure 1). This approach is particularly interesting since it combines the advantages of both generic and parametric modelings. It is:

- **robust:** the robustness of parametric approaches is preserved since all objects of the grammar are defined through a set of parameters.
- **generic:** a grammar of quality allows to reconstruct a large range of buildings. It is even possible to reconstruct buildings that some generic modelings cannot such as the curved roof structures.

However, this approach is based on an important prior knowledge concerning urban structures and their assembling. It is necessary to correctly define these structure interactions in order to have a satisfactory modeling without artefact.
We present below a 3D city modeling based on such an approach from a single input well adapted to geometric description: the DEM. It is composed of an extraction step followed by a 3D reconstruction step presented in the next sections.

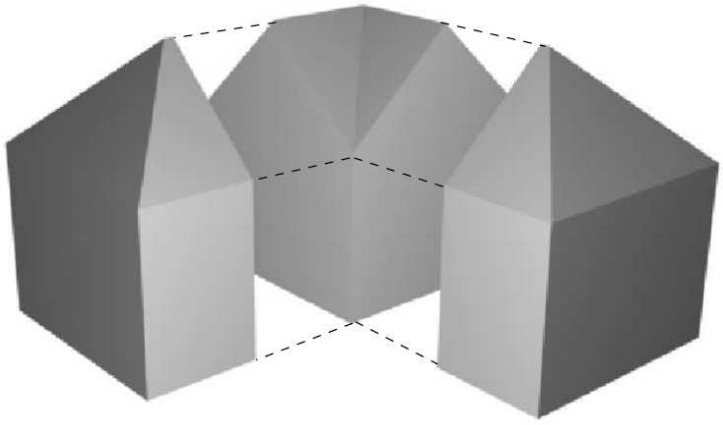

Figure 1: Principle of the structural approach

1.2.2 Footprint extraction

The first step consists in extracting the building footprints from DEMs through configurations of polygons, more precisely configurations of connected quadrilaterals (i.e. quadrilaterals with common edges). Each one is a specific part of a building. In the structural approach, these quadrilaterals correspond to the base of the simple urban structures. Some quadrilateral edges can represent facade discontinuities. This process has been presented in previous works [15] [17] and will not be detailed in this report. Figure 2 shows examples of obtained building footprints.

1.2.3 3D reconstruction

The second step corresponds to the 3D reconstruction using both DEMs and obtained building footprints. In this report, we focus on this part.
Firstly, we propose a grammar of 3D-models adapted to the urban landscape. Secondly, an energy formulation is used in a Bayesian expression. This framework is particularly well adapted to introduce prior knowledge concerning urban structures and their assembling. Then, two different optimization processes which allow to minimize this energy (a RJMCMC algorithm and a Viterbi algorithm) are detailed and compared. Finally, results on PLEIADES simulations are presented.

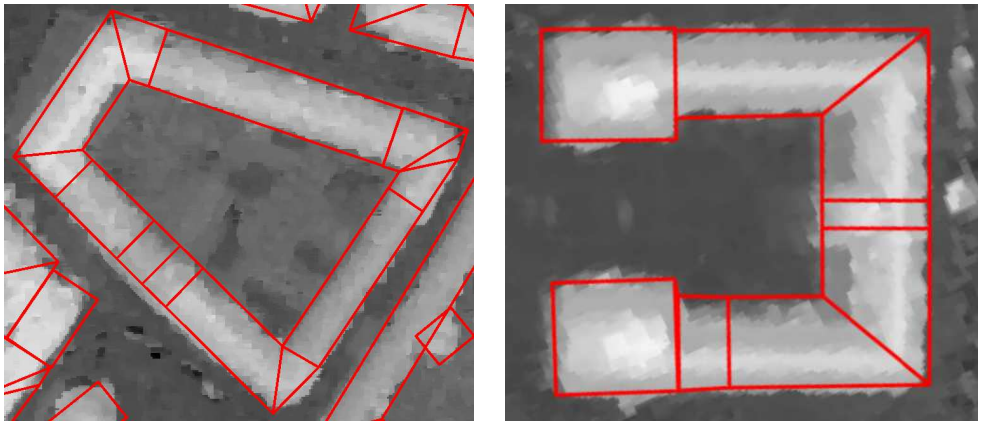

(a) (b)

Figure 2: **(a)&(b):** Examples of obtained building footprints with DEMs from PLEIADES simulations (©INRIA/CNES/IGN).

2 Grammar of 3D-models

In this section, we establish a grammar of 3D-models which is representative of the French urban landscape.

2.1 Description of the urban landscape

Figure 3 reminds some terms concerning roofs useful in the understanding of the report. There are various factors which influence the building morphology, especially the morphology of the roofs:

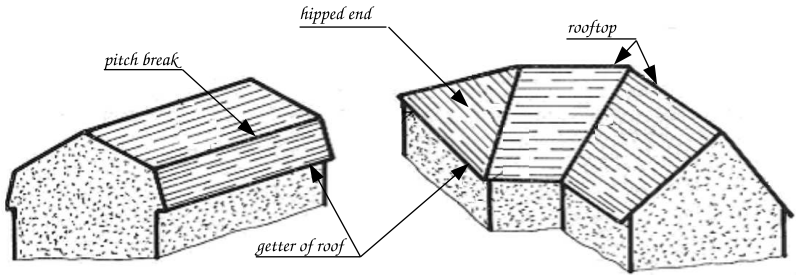

Figure 3: Some roof terms

- **Climatic influences**: The climate of an area is a determining factor in the morphology of the roofs. For example, rainfall areas will favor the presence of strong slope roofs. In the same way, strong winds contribute to the development of multi-plane roofs.
- **Social influences**: Cities are constructed according to social schemes. Several kinds of urban areas can be distinguished such as the downtowns, the suburban areas or the industrial parks. The roof morphology is strongly linked to these kinds of areas. For example, industrial parks contain many flat roof buildings whereas multi-plane roofs of high volumes such as gambrel are favored in downtowns in order to optimize livable space.

These factors allow to determine the most common roof types and to classify them.

2.2 The most common roofs and their modelings

In this paragraph, we present a collection of roofs which is representative of a majority of urban landscape[1]. These roofs are modeled by a set of parameters knowing the quadrilateral footprints[2].

Table 1 presents the parameters used to model the various roofs. The parameters H_t, H_g and ψ are used in the majority of models. The parameter η appears when a model owns at least one hipped end. Figure 4 presents a description of both parameters ψ and η. The roofs can be classified according to three types: the monoplanes, the multi-planes and the curved roofs.

H_t	rooftop height	in $[H_{tmin}, H_{tmax}]$
H_g	getter of roof height	in $[H_{gmin}, H_{gmax}]$
ϕ	orientation of the roof w.r.t. the quadrilateral base	in $\{1, 2, 3, 4\}$
η	positioning of the hipped end w.r.t. the quadrilateral base	in $[0, 1]$
ζ	positioning of the rooftop w.r.t. the quadrilateral width	in $[0, 1]$
κ	positioning of the pitch break w.r.t. the quadrilateral base	in $[0, 1]^2$
ξ	positioning of the platform w.r.t. the quadrilateral base	in $[0, 1]^4$

Table 1: parameters defining the roofs

[1] More precisely, this collection of roofs is well adapted to "developed countries", especially Europe and U.S.A.

[2] The following 3D-models are shown with a rectangular base but, in practice, the base is an unspecified quadrilateral (or even a triangle).

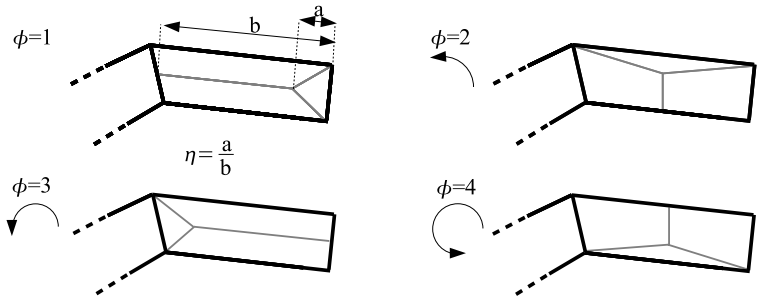

Figure 4: Description of parameters ψ and η

2.2.1 The monoplanes

	3D view	top & profile	models	parameters
flat roof	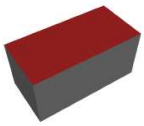	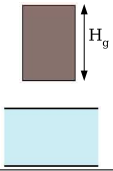	$\mathcal{M}_{110}$: 	H_g
platform roof	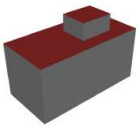	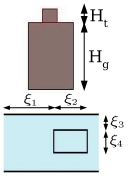	$\mathcal{M}_{120}$: 	H_g,H_t,ξ_1, ξ_2,ξ_3,ξ_4,ϕ
shed roof	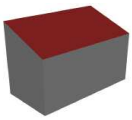	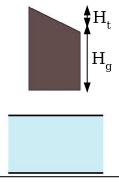	$\mathcal{M}_{130}$: 	H_g, H_t, ϕ

2.2.2 The multi-planes

	3D view	top & profile	models	parameters
gable roof	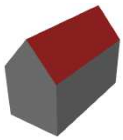	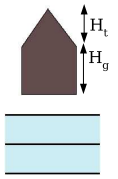	$\mathcal{M}_{210}$:  $\mathcal{M}_{211}$:  $\mathcal{M}_{212}$: 	H_g, H_t, ϕ $+\eta$ ($\mathcal{M}_{211}$ & $\mathcal{M}_{212}$)
dissymmetric gable roof		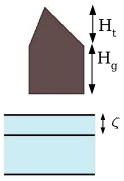	$\mathcal{M}_{220}$:  $\mathcal{M}_{221}$:  $\mathcal{M}_{222}$: 	H_g, H_t, ζ, ϕ $+\eta$ ($\mathcal{M}_{221}$ & $\mathcal{M}_{222}$)
saltbox roof		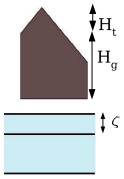	$\mathcal{M}_{230}$:  $\mathcal{M}_{231}$:  $\mathcal{M}_{232}$: 	H_g, H_t, ζ, ϕ $+\eta$ ($\mathcal{M}_{231}$ & $\mathcal{M}_{232}$)
gambrel roof	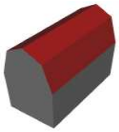	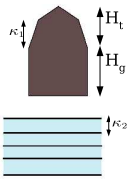	$\mathcal{M}_{240}$:  $\mathcal{M}_{241}$:  $\mathcal{M}_{242}$: 	$H_g, H_t, \kappa_1,$ κ_2, ϕ $+\eta$ ($\mathcal{M}_{241}$ & $\mathcal{M}_{242}$)
mansard roof	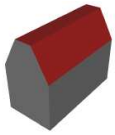	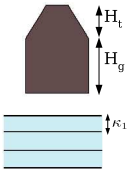	$\mathcal{M}_{260}$:  $\mathcal{M}_{261}$:  $\mathcal{M}_{262}$: 	H_g, H_t, κ_1, ϕ $+\eta$ ($\mathcal{M}_{261}$ & $\mathcal{M}_{262}$)

2.2.3 The curved roofs

	3D view	top & profile	models	parameters
$\frac{1}{2}$-elliptic roof	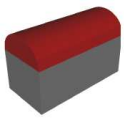	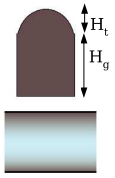	$\mathcal{M}_{310}$:  $\mathcal{M}_{311}$:  $\mathcal{M}_{312}$: 	H_g, H_t, ϕ $+\eta$ ($\mathcal{M}_{311}$ & $\mathcal{M}_{312}$)
$\frac{1}{4}$-elliptic roof	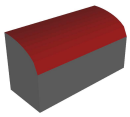	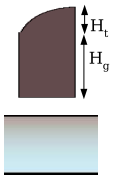	$\mathcal{M}_{320}$: 	H_g, H_t, ϕ

2.3 Contents of grammars with respect to the data quality

The use of the previous 3D-models in reconstruction process depends on the data resolution. Aerial image resolution is, in the general, high enough to make the distinction between all these kinds of roofs. However, it is not the case for the satellite data and more precisely PLEIADES simulations. Therefore, it is necessary to estimate the potential of these data in order to select the models which will constitute the grammar. Figure 5 represents various

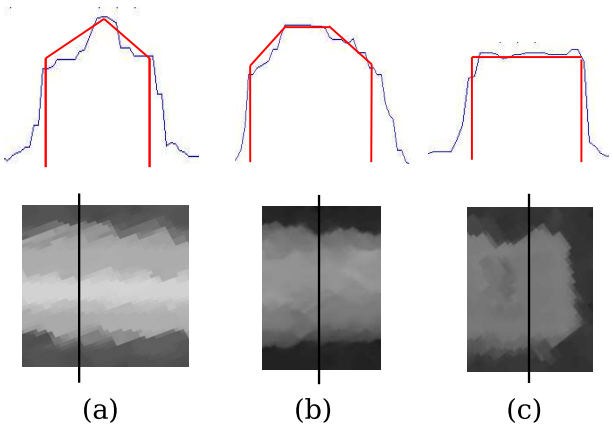

Figure 5: Various building profiles on satellite DEM (blue) associated with the real profiles (red).

building profiles of satellite DEMs. First, the PLEIADES data allow to distinguish the positioning of the rooftop along the footprints (profile (a)). As a consequence, the dissymmetric roof models ($\mathcal{M}_{22x}$ and $\mathcal{M}_{23x}$) can be included into the grammar. Then, flat structures are correctly restored as we can see with the profiles (b) and (c). The grammar can contain $\mathcal{M}_{1xx}$ and $\mathcal{M}_{26x}$ models. However, profiles (b) and (a) show that pitch breaks cannot be clearly distinguished, that means $\mathcal{M}_{24x}$ models must be excluded.

To sum-up, the selected grammar for PLEIADES data $\mathcal{M}$, presented in Figure 6, is composed of the following 3D-models:

$$\mathcal{M} = \{\mathcal{M}_{1xx}, \mathcal{M}_{21x}, \mathcal{M}_{22x}, \mathcal{M}_{23x}, \mathcal{M}_{26x}, \mathcal{M}_{3xx}\} \quad (1)$$

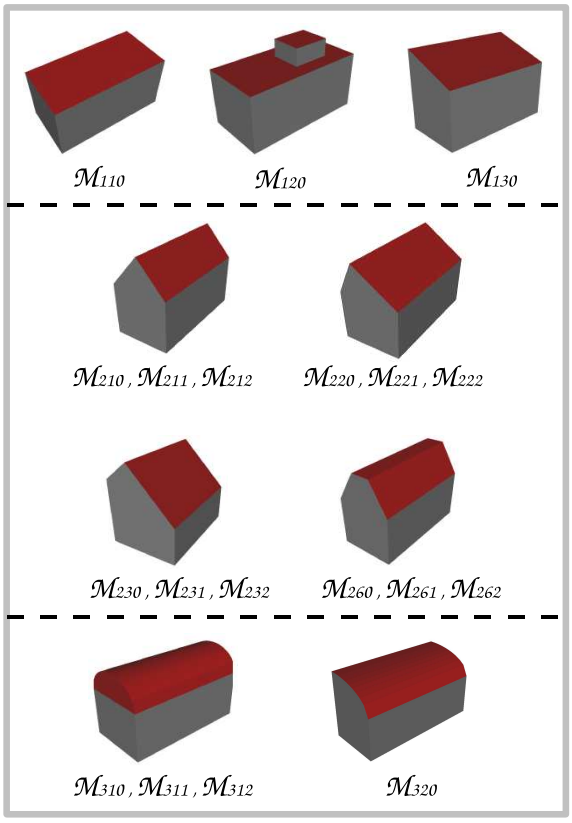

Figure 6: The grammar $\mathcal{M}$ of 3D-models for PLEIADES data.

Each model $\mathcal{M}_m \in \mathcal{M}$ has a number of parameters which is varying from 1 (for model $\mathcal{M}_{110}$) to 7 (for the model $\mathcal{M}_{120}$) .

3 Energy formulation

The energy formulation developed in this section requires a substantial amount of notation, summarized below :

- S, a set of sites and $I = \{\Lambda_s / s \in S\}$, a given DEM where Λ_s represents the intensity of the site s,
- $\mathcal{Q}$, the object space of a quadrilateral with marked edges,
- $\mathcal{C} \in \mathcal{Q}^N$, the quadrilateral configuration representing the building footprints associated with I where N represents the number of quadrilaterals (see Figure 2),
- S_i, the subset of S whose sites are inside the quadrilateral $i \in \mathcal{C}$,
- $\mathcal{D} = \{\Lambda_s \in I / s \in S_i \, , i \in \mathcal{C}\}$, the set of data,
- $\mathcal{D}_i = \{\Lambda_s \in I / s \in S_i\}$, the partial data of the quadrilateral i,
- x, an element of the state space $\mathcal{T}$ which corresponds to a configuration of 3D-parametric objects knowing the quadrilateral footprints $\mathcal{C}$.
  $x = (x_i)_{i \in \mathcal{C}} = (m_i, \theta_i)_{i \in \mathcal{C}}$ where each object x_i is defined by both a roof type $\mathcal{M}_{m_i} \in \mathcal{M}$ and a set of parameters θ_i associated with $\mathcal{M}_{m_i}$. In the following, $x_i = (m_i, \theta_i)$ and $\mathcal{M}_{m_i}$ will be respectively called an object and a model,
- d_m, the number of parameters of the model $\mathcal{M}_m$,
- $\mathcal{S}_{x_i}$, the function from S_i to $\mathbb{R}$ which associates the roof altitude of the object x_i to each site of S_i.

3.1 Bayesian framework

The Bayesian framework is especially well adapted to our problem since it allows to introduce a priori knowledge concerning models and their assembling. Moreover, this framework is known to have interesting properties concerning the parameter estimation problem.

Let us consider the measurable spaces $(\Omega_k, \mathcal{A}_k, \upsilon_k)$ associated with the Lebesgue measure on $\mathbb{R}^k$ where $k \in \mathbb{N}^\star$.
The measure associated with the parameters of a model $\mathcal{M}_m \in \mathcal{M}$ is then given by :

$$\mu(x) = \sum_{k \in \mathbb{N}^\star} \mathbb{1}_{\{m=k\}} \nu_{d_k}(\theta) \tag{2}$$

Let us now consider the measurable space $(\mathcal{T}, \mathcal{B}(\mathcal{T}), \mu(.)^N)$ related to the state space $\mathcal{T}$ where $\mu(.)^N$ is the product measure of $\mu(.)$. We consider the random variable X distributed in $\mathcal{T}$ which follows an unnormalized density $h(.)$ against $\mu(.)^N$. $h(.)$ is actually the posterior density of a configuration of objects x, given $\mathcal{D}$. In a Bayesian framework, this density can be expressed as follows :

$$h(x) = h(x/\mathcal{D}) \propto \mathcal{L}(\mathcal{D}/x) h_p(x) \tag{3}$$

$\mathcal{L}(\mathcal{D}/x)$ is the likelihood. It represents the probability of observing the data $\mathcal{D}$ knowing the configuration x. $h_p(x)$ is the prior density which allows to take into account interactions existing between models. A requirement is to be able to build both $h_p(x)$ and $\mathcal{L}(\mathcal{D}/x)$.

To do so, the Gibbs formulation is used [3]. It consists in expressing an unnormalized density $h(.)$ by using an energy U thanks to the following equation :

$$h(x) = \exp -U(x) \tag{4}$$

To sum-up, the posterior density $h(.)$ can be expressed as follows :

$$h(.) = \exp -(U_d + U_p) \tag{5}$$

where U_d and U_p are Gibbs energies associated with $\mathcal{L}(.)$ and $h_p(.)$ respectively. In the following, these two terms are detailed.

3.2 Likelihood

The data $\mathcal{D}$ and the partial data $\mathcal{D}_i$ are linked $\mathcal{D} = \bigcup_{i \in \mathcal{C}} \mathcal{D}_i$. By considering the hypothesis of conditional independence (which is verified since the covering of quadrilateral is null), the likelihood can be expressed as :

$$\mathcal{L}(\mathcal{D}/x) = \prod_{i \in \mathcal{C}} \mathcal{L}(\mathcal{D}_i/x_i) = \exp - \sum_{i \in \mathcal{C}} U_d^{(i)}(x_i) \tag{6}$$

$\mathcal{L}(\mathcal{D}_i/x_i)$ represents the probability of observing $\mathcal{D}_i$ knowing the configuration x_i and can be expressed using a partial data energy $U_d^{(i)}$.

Let us consider $\Gamma^{\alpha}_{(i)}(.,.)$, the distance from $\mathbb{R}^{card(S_i)} \times \mathbb{R}^{card(S_i)}$ to $\mathbb{R}$ defined by :

$$\forall (x,y) \in \mathbb{R}^{card(S_i)} \times \mathbb{R}^{card(S_i)}, \alpha \in \mathbb{R}^{\star +}, \Gamma^{\alpha}_{(i)}(x,y) = \left(\sum_{s \in S_i} |x_s - y_s|^{\alpha} \right)^{\frac{1}{\alpha}} \tag{7}$$

[3] The common Gibbs formulation deals with a normalized density. The equation (4) is then given by $h(x) = \frac{1}{Z} \exp(-U(x))$ where Z is a normalizing constant defined by $Z = \int_{x \in \mathcal{T}} \exp -U(x)$.
However, this normalizing constant cannot be easily computed or estimated since the state space dimension is very large. That is why we prefer to use an unnormalized density with an adapted optimization method such as the MCMC algorithm which is described in section 4.1.

The partial data energy $U_d^{(i)}$ is then defined through the distance $\Gamma_{(i)}^{\alpha}(.,.)$ by the following expression :

$$U_d^{(i)}(x_i) = \Gamma_{(i)}^{\alpha}(\mathcal{S}_{x_i}, \mathcal{D}_i) \tag{8}$$

So, the partial data energy $U_d^{(i)}$ corresponds to the Z-error of the L_α norm between the DEM and the object x_i. In practice, we choose $\alpha = 1.2$.

The likelihood is given by :

$$\mathcal{L}(\mathcal{D}/x) = \exp - \sum_{i \in \mathcal{C}} \Gamma_{(i)}^{\alpha}(\mathcal{S}_{x_i}, \mathcal{D}_i) \tag{9}$$

3.3 A priori

The a priori energy is a key point in the structural approach. This term allows to correctly assemble objects in order to propose a realistic building.

To do so, the prior energy is defined through interactions between objects (i.e. energies of second-order $U(x_i, x_j)$ where i, j are neighboring elements of the quadrilateral configuration $\mathcal{C}$). It allows to favor some assemblings and penalize other ones.

In previous our work [16], too many interactions have been set up. The number of terms in the prior must be minimal in order to keep robustness and avoid problems of parameter settings. In other words, we want an prior energy which is simple and efficient.

In order to correctly assemble the various urban structures, the prior energy must take into account both altimetric and morphological interactions. The altimetric interaction has to adjust the rooftop and getter of roof heights between neighboring elements. The morphological interaction must favor the continuity of the roof form between neighboring elements.

3.3.1 neighborhood relationship

A neighborhood relationship on $\mathcal{C}$ must be set up in order to define the interactions. Two elements are neighbor if they verify the following points :

- both quadrilaterals must have a common edge,
- the common edge must not be a facade discontinuity (see section 1.2.2).

Definition 1 (neighborhood relationship ν) *Let us consider two distinct quadrilaterals i and $j \in \mathcal{C}$. j is said neighbor of i if and only if the quadrilaterals i and j have one common edge which is not a facade discontinuity.*
The neighborhood relationship is noticed $\bowtie$. $i \bowtie j$ represents the set of neighbor pairs of $\mathcal{C}$.

3.3.2 "joinable" objects

All the models of $\mathcal{M}$ cannot be assembled together. For example, it is not possible to merge a curved roof with a mansard roof. So, it is necessary to define an assembling law. Two objects $x_i = (m_i, \theta_i)$ and $x_j = (m_j, \theta_j)$ will be said "**joinable**" if and only if:

- models $\mathcal{M}_{m_i}$ and $\mathcal{M}_{m_j}$ belong to the same assembling family defined in the table 2,
- orientation parameters ϕ_i and ϕ_j are the same.

This relation is noticed $x_i \sim_a x_j$.

Families of "joinable" objects	set of common parameters $\theta^\star$
$\mathcal{M}_{110}, \mathcal{M}_{120}$	H_g
$\mathcal{M}_{210}, \mathcal{M}_{211}$	H_g, H_t
$\mathcal{M}_{220}, \mathcal{M}_{221}$	H_g, H_t, ζ
$\mathcal{M}_{230}, \mathcal{M}_{231}$	H_g, H_t, ζ
$\mathcal{M}_{240}, \mathcal{M}_{241}$	H_g, H_t, κ_1, κ_2
$\mathcal{M}_{260}, \mathcal{M}_{261}$	H_g, H_t, κ_1
$\mathcal{M}_{310}, \mathcal{M}_{311}$	H_g, H_t

Table 2: Families of the joinable objects.

The models which do not appear in the table 2 are roof types which cannot be assembled: they are not "joinable" with any other including themselves.

3.3.3 prior energy

The prior energy consists in favoring the "joinable" objects. More precisely, in order to avoid the artefacts, we want to favor the set of common parameters $\theta^\star$ (defined in the table 2) of two "joinable" objects. To do so, the following energy is used.

$$\forall x \in \mathcal{T},\ U_p(x) = \beta \sum_{i \bowtie j} \mathbb{1}_{\{x_i \sim_a x_j\}} g(x_i, x_j) \tag{10}$$

where $\beta \in \mathbb{R}^+$ is the parameter which weights the importance of the prior density with respect to the likelihood. The function g, living in $[-1, 0]$, measures the distance between the common parameters of two "joinable" objects.

$$g(x, x') = \frac{D(x, x')}{D_{max}} - 1 = \frac{\sum_{k=1 \ldots d^\star} \omega_k |\theta^\star_{(k)} - \theta'^\star_{(k)}|}{D_{max}} - 1 \tag{11}$$

The parameters of a model can correspond to altimetric and morphological criteria. That is why it is necessary to introduce weights ω_k in this distance in order to normalize the metric

associated with the different parameters. These weights are computed knowing the XY and Z resolutions and the configuration of quadrilaterals $\mathcal{C}$.
$d^\star$ is the number of parameters of $\theta^\star$, and D_{max} represents the maximum value of the distance : $D_{max} = \max_{x,x'} D(x, x')$.

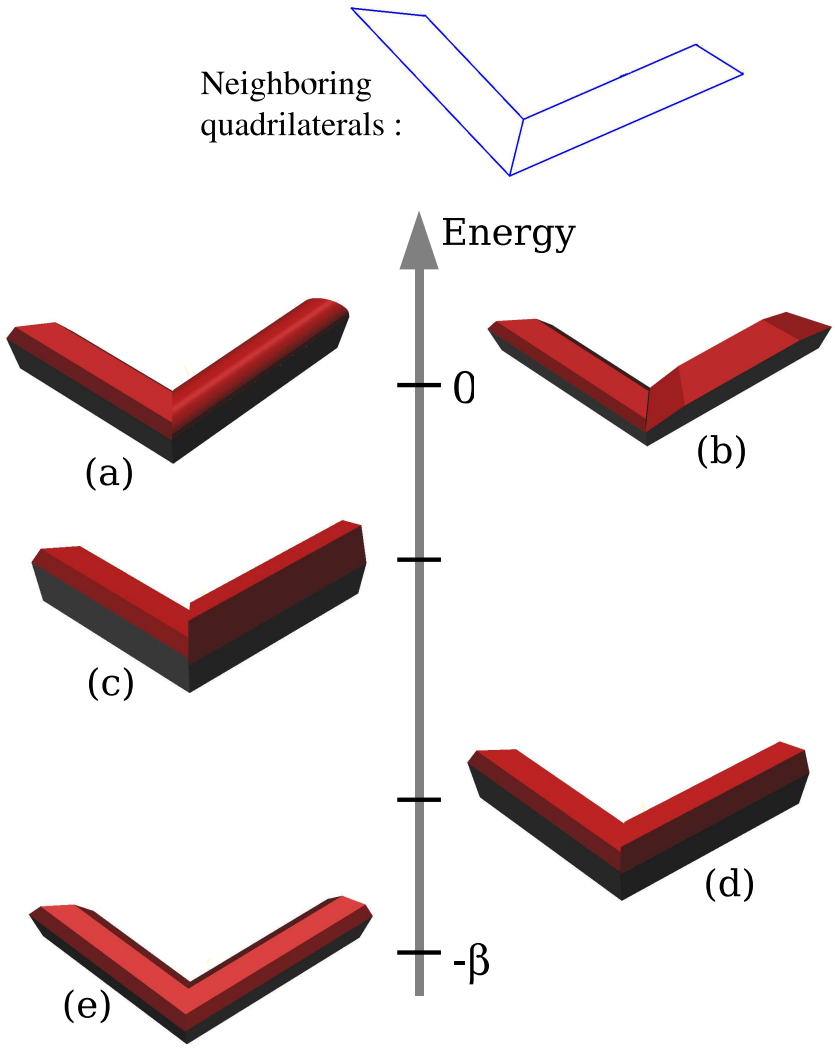

Figure 7: Principle of the prior energy - examples of various interaction cases.

Figure 7 shows the principle of this interaction. If the two models belong to different families of "joinable" objects (for example a mansard roof model and a semi-elliptic roof model in figure 7-(a)) or if the two objects do not have the same orientation parameter ϕ (in figure 7-(b) : the two objects are mansard roofs with the same set of parameters except for ϕ), they will not be "joinable" and so, the energy will be null. Now, if the two objects are "joinable" (figure 7-(c)-(d)-(e)), the energy will be negative : these configurations are favored. The nearer the parameters of the two objects, the lower the energy. The configuration (e) is the best one.

4 Optimization

We aim at finding the configuration of objects which maximizes the posterior density $h(.)$. We search for the Maximum A Posteriori (MAP) estimator x_{MAP}:

$$x_{MAP} = \arg\max_{x} h(x) \tag{12}$$

This is a non convex optimization problem in a high and variable dimension space $\mathcal{T}$ since the models of collection $\mathcal{M}$ are defined by a different number of parameters.
This optimization step is tackled by two different methods detailed in below.

4.1 RJMCMC algorithm

The Reversible Jump Markov Chain Monte Carlo (RJMCMC) algorithm [8] [25] is a stochastic optimization method which is well adapted to our problem. This technique is an extension of the formalism introduced by Hastings [12] which allows to deal with variable dimension state spaces. Several papers such as [2] have shown the efficiency of the RJMCMC sampler for the methods based on multiple parametric object recognition.

It consists in simulating a discrete Markov Chain $(X_t)_{t\in\mathbb{N}}$ on $\mathcal{T}$ having π as invariant measure (specified by the posterior density $h(.)$) which performs small jumps between spaces of variable dimensions respecting the reversibility assumption of the chain. Propositions are based on “small jumps” which means only one object of the global configuration will be concerned by a new proposition. One of the main advantages of such a sampler is that the chain asymptotically converges towards π for all initial configuration x_0.

Let us consider two models $\mathcal{M}_m$ and $\mathcal{M}_n$ and a move (or jump) from $x_i = (m, \theta_i)$ to $\widehat{x_i} = (n, \widehat{\theta_i})$. The idea of Green is to create a bijection between the parameter spaces of the models $\mathcal{M}_m$ and $\mathcal{M}_n$. θ_i is completed by a simulation $u_{mn} \sim \varphi_{mn}(.)$ into (θ_i, u_{mn}), and $\widehat{\theta_i}$ by $v_{nm} \sim \varphi_{nm}(.)$ into $(\widehat{\theta_i}, v_{mn})$ such as the mapping Ψ_{mn} between (θ_i, u_{mn}) and $(\widehat{\theta_i}, v_{mn})$ is a bijection :

$$(\widehat{\theta_i}, v_{mn}) = \Psi_{mn}(\theta_i, u_{mn}) \tag{13}$$

The probability of acceptance for the move from x_i to $\widehat{x_i}$ is then given by:

$$\min\left(\frac{\pi(\widehat{x})}{\pi(x)}\frac{J_{nm}\varphi_{nm}(v_{nm})}{J_{mn}\varphi_{mn}(u_{mn})}\left|\frac{\partial\Psi_{mn}(\theta_i,u_{mn})}{\partial(\theta_i,u_{mn})}\right|,1\right) \tag{14}$$

where J_{mn} is the probability of choosing a jump to $\mathcal{M}_n$ while in $\mathcal{M}_m$ and φ_{mn}, the density of u_{mn} (here, the u_{mn} follow uniform distributions).

Finding the bijection Ψ_{mn} is a difficult problem when $\mathcal{M}_m$ and $\mathcal{M}_n$ differ from many dimensions [25]. In practice, the jumps are limited to moves from $\mathcal{M}_m$ to models with close dimensions. It is the case in our problem: the models of the grammar $\mathcal{M}$ differ from few dimensions. The jumps from any model to any other one are then allowed.

The RJMCMC sampler can be resumed as follows :

Algorithm 1 (RJMCMC sampler)
At iteration t, if $x^{(t)}=(m,\theta)$,

- *select model* $\mathcal{M}_n$ *with probability* J_{mn}
- *generate* $u_{mn}\sim\varphi_{mn}(u)$
- *set* $(\widehat{\theta},v_{mn})=\Psi_{mn}(\theta,u_{mn})$
- *take* $x^{(t+1)}=(n,\widehat{\theta})$ *with probability*

$$\min\left(\frac{\pi(n,\widehat{\theta})}{\pi(m,\theta)}\frac{J_{nm}\varphi_{nm}(v_{nm})}{J_{mn}\varphi_{mn}(u_{mn})}\left|\frac{\partial\Psi_{mn}(\theta,u_{mn})}{\partial(\theta,u_{mn})}\right|,1\right)$$

and take $x^{(t+1)}=x^{(t)}$ *otherwise.*

In practice, a simulated annealing, introduced by [20], is used : the density $h(.)$ is substituted by $h(.)^{\frac{1}{T_t}}$ where T_t is a sequence of temperatures which tends to zero as t tends to infinity. At the beginning of the algorithm (i.e. when the temperature is high), the process is not really selective : it allows to explore the density modes. When the temperature decreases, configurations which have a high density are favored.

Temperature decrease

The simulated annealing generates parameters. The first point consists in choosing the type of cooling schedule. A logarithmic decrease allows to ensure the algorithm convergence. However, this cooling schedule requires too much computation time and is not usable in practice. Even if we are bound to lose the convergence conditions, we prefer implementing some faster cooling schedules. We use a geometrical decrease defined as follows:

$$T_t = T_o.\alpha^t \tag{15}$$

where $\alpha < 1$ and close to 1 and T_0 is the initial temperature.
This cooling schedule allows to provide an approximate solution close to the optimal one in faster computing time. More details concerning this cooling schedule are available in [30]. In addition, there are faster cooling schedules which consist in adapting the temperature decrease according to the variation of the energy [11][22][31]

The two main parameters are the initial and ending temperatures T_0 and T_{final}. Generally speaking, the cooling schedule should take into account the energy to be optimized, its scale, its landscape, the number and the size of local minima (see [27]).

- Choice of T_o
  [35] suggests to link the initial temperature T_0 with the variation of the energy U on random configurations. More precisely, T_0 is chosen as at least twice the standard deviation of U at infinite temperature :

  $$T_0 \geq 2.\sigma(E_{T=\infty}) = 2.\sqrt{\langle E^2_{T=\infty}\rangle - \langle E_{T=\infty}\rangle^2} \tag{16}$$

  where $\langle E\rangle$ is the means of the energy of the samples. In practice, we take $T_0 = 2.\sigma(E_{T=\infty})$ and we estimate it by randomly sampling the state space (several thousand samples are necessary to obtain a good estimation - it is negligible w.r.t. the number of iterations of the optimization process).

- Choice of T_{final}
  The ending temperature T_{final} must depend on the variation of the energy too. A usual choice consists in stopping the algorithm when the energy does not change during a certain number of iterations. [35] proposes another idea in taking T_{final} of the order of the smallest energy scale (i.e. taking the smallest possible energy variation ΔE of a single move). Discrete problems allow to estimate T_{final} for an easier way.

Figure 8 shows an example of a simulation of such a cooling schedule on the Amiens city hall (France). T_0 has been normalized to the value 1 on the results. When the temperature is high, the process explores the density modes : the building is composed of all kinds of 3D-models. At $t = 10^{-2}$, the process begins to be selective and the building is structured. At low temperature, the configuration is close to the optimal solution and does not evolve very

much : it consists in a detailed adjustment of the 3D-models which compose the building. The computing time is 156 seconds on a 3Ghz processor to get the final result shown for $T = 5.10^{-6}$.

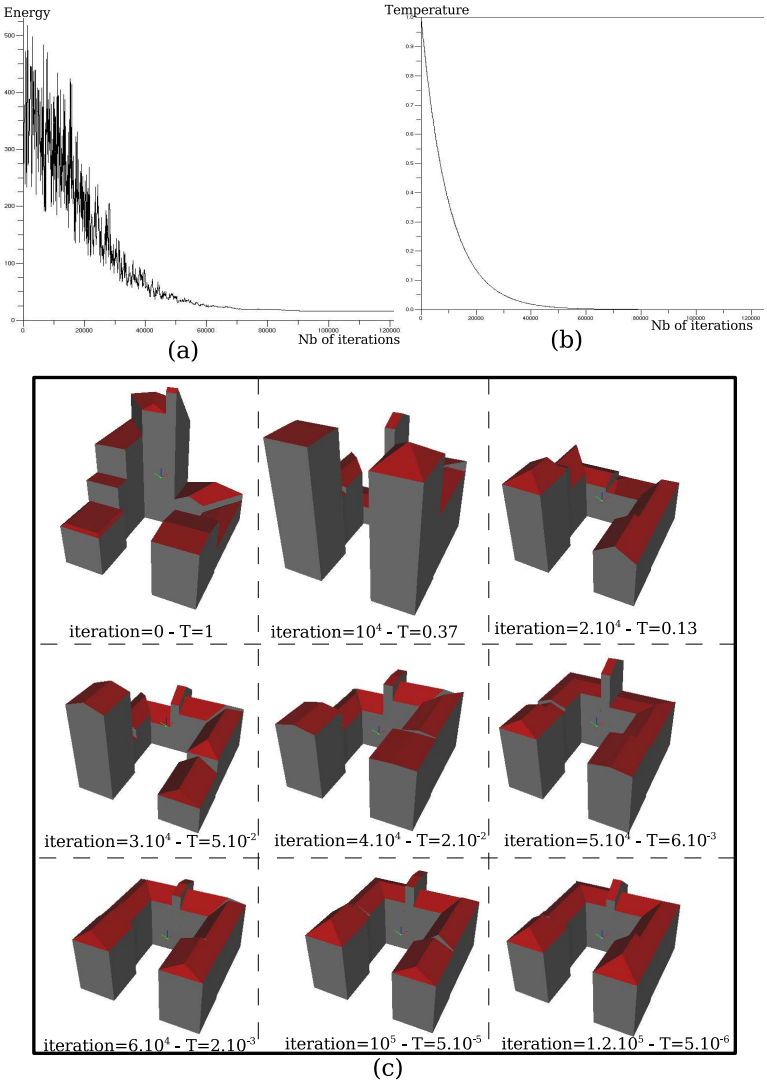

Figure 8: Example of a simulation on the Amiens city hall (France) **(a)**- Energy decrease in function of the number of iterations **(b)** Temperature decrease in function of the number of iterations **(c)**- Samples of configurations at different temperatures.

4.2 Viterbi algorithm

The Viterbi algorithm [4][33] is a deterministic optimization method used, first, in the dynamic programming framework and then in speech recognition [24] and image processing [21]. It allows to find the optimal path through a Hidden Markov Model (HMM).

Let us consider $(X_t, Y_t)_{t=1}^T$, a homogeneous hidden Markov chain where $X = (X_t)_t$ represents the hidden states and $Y = (Y_t)_t$ corresponds to the sequence of observations. The transition probabilities are defined as $a_{ij} = P(X_{t+1} = j | X_t = i)$. Y is supposed to be independent with respect to X. Figure 9 represents the dependence graph of this chain.

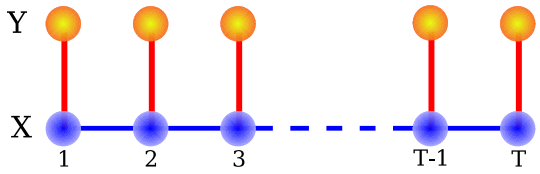

Figure 9: Dependence graph of the hidden Markov chain $(X_t, Y_t)_{t=1}^T$

Let us consider $\delta_t(i)$, the probability of the optimal path which allows to reach the state i at the time t knowing the observations Y. In other words, $\delta_t(i)$ is the MAP probability of the "sub-chain" ending at t with X_t fixed.

$$\delta_t(i) = \max_{x_1,...,x_{t-1}} P(y_1, ..., y_{t-1}, X_1 = x_1, ..., X_{t-1} = x_{t-1}, X_t = i) \tag{17}$$

By a recurrence relation, we can determine the δ_{t+1} in function of the δ_t :

$$\begin{aligned}
\delta_{t+1}(j) &= \max_{x_1,...,x_t} P(y_1, ..., y_t, X_1 = x_1, ..., X_t = x_t, X_{t+1} = j) \\
&= \max_{x_t} \left[P(X_{t+1} = j | X_t = x_t) \max_{x_1,...,x_{t-1}} P(y_1, ..., y_t, X_1 = x_1, ..., X_t = x_t) \right] \\
&= \max_i \left[a_{ij} P(y_t | X_t = i) \max_{x_1,...,x_{t-1}} P(y_1, ..., y_t, X_1 = x_1, ..., X_{t-1} = x_{t-1}, X_t = i) \right]
\end{aligned}$$

We obtain the following relation :

$$\delta_{t+1}(j) = \max_i \left[a_{ij} \mathcal{L}_i(y_t) \delta_t(i) \right] \tag{18}$$

where $\mathcal{L}_i(y_t) = P(y_t | X_t = i)$ represents the local likelihood of the t^{th} element of the chain. The argument which gives the maximum is noted $\Psi_{t+1}(j)$:

$$\Psi_{t+1}(j) = \arg\max_i \left[a_{ij} \mathcal{L}_i(y_t) \delta_t(i) \right] \tag{19}$$

The Viterbi algorithm can be described as follows :

Algorithm 2 (Viterbi algorithm)

- *At* $t = 1$ *: initialize* $\delta_1(i) = P(X_1 = i)$, $\forall i$.
- *For* $t = 2...T$ *: compute and keep in a table the couples* $(\delta_t(j), \Psi_t(j))$, $\forall j$.
- *compute the MAP given by :* $\widehat{x}_T = \arg\max_i \mathcal{L}_i(y_T)\delta_T(i)$
- *read the optimal path in the table given by :* $\widehat{x}_t = \Psi_{t+1}(\widehat{x}_{t+1})$, *for* $t = T-1, ..., 1$

How to adapt our problem to this HMM ?

- A building footprint as a sequences of objects
  The Viterbi algorithm deals with sequences of objects. In our case, an object is a 3D-model associated with a quadrilateral footprint. It means that a building footprint must form a sequence of quadrilaterals. This constraint has been studied in our previous works [15] [17] where pre-processing have allowed to morph a collection of quadrilaterals associated with a building into a quadrilateral sequence and isolated quadrilaterals.

- link between the energy formulation and the HMM
  The Viterbi algorithm has been previously formalized using probabilities (i.e. normalized densities). However, this algorithm allows to deal with unnormalized densities such as $h_p(.)$ and $\mathcal{L}(.)$ defined in the previous section. So, if we search for the MAP of $h(.)$, the transition probabilities a_{ij} correspond to the prior density $h_p(x)$ where $x = (i, j)$ and the local likelihood $\mathcal{L}_i(y_t)$ are given by $\mathcal{L}(\mathcal{D}_t|i)$. To sum-up, we have:

$$a_{ij} \propto \exp -U_p(i, j) \tag{20}$$

$$\mathcal{L}_i(y_t) \propto \exp -U_d(i) \tag{21}$$

- State space discretization
  The Viterbi technique is an exhaustive search algorithm. The computing time is then directly linked to the size of the state space. It is necessary to discretize it in order to have correct computing time and to avoid problems of memory saturation. Figure 10 shows results obtained from different discretization steps of the state space. The discretization step, which is linked to a precision degree (in meter) of the result w.r.t. the data, must be compared to the computing time. In figure 10 - (a), the discretization step is high (2.5 meters) : the result is not precise but the computing time is very short (1 second). On the contrary, in figure 10 - (c), the result is very precise

(the discretization step is 0.2 meter) but the computing time is very high (nearly 13 hours). Taking a 0.1 meter discretization step engenders memory saturation problems. As a consequence, it is interesting to use the Viterbi algorithm in order to obtain an approximate solution (i.e. with a high discretization step) with short computing time.

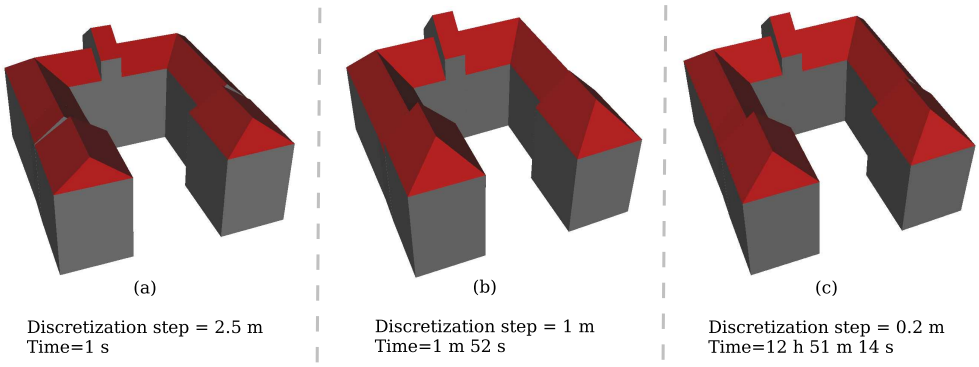

Figure 10: Results on the Amiens city hall (France) obtained by the Viterbi algorithm with different discretization steps of the state space.

4.3 Comments

These two optimization methods differ from many points. The choice of the method depends on the following dilemma: accuracy of the results VS computing time. Let us recall the advantages and drawbacks of each technique:

- RJMCMC algorithm
  This stochastic method allows to theoretically find the optimal solution. In practice (i.e. using a non logarithmic cooling schedule), it provides a very good solution close to the optimal one. However, the computing time is quite high. This last point can be improved by proposing adaptive cooling schedules.

- Viterbi algorithm
  It is a deterministic method which allows to provide the optimal solution with respect to the state space. In practice, the state space must be strongly discretized in order to have interesting computing time. Moreover, this algorithm imposes constraints of causality on the object layout which must be presented as a sequence.

So, in our application, they must be seen as complementary optimization methods depending on the user context. The RJMCMC algorithm has to be used to obtain a very

good solution, close to the optimal one without having time constraints. On the contrary, the Viterbi algorithm must be implemented to provide an approximate solution (which can be far away from the optimal one since the state space is strongly discretized) in short computing time.

5 Results

The results have been obtained from PLEIADES simulations on Amiens city (France). DEMs have been generated by a method based on a multi-resolution implementation of a Cox and Roy optimal flow matching image algorithm [26]. More details concerning the DEM generation can be found in [23]. The RJMCMC algorithm has been used to provide the following 3D results. It has been preferred to the Viterbi algorithm in order to have an accurate solution which allows to estimate the energy quality.

Figures 11 and 12 present some examples of reconstructed buildings associated with the PLEIADES simulation and the building footprints. These results are in general satisfactory. Some details are omitted as we can see on some examples. It is due to both the average quality of the data and the limits of the proposed method in term of genericity. However, the global shape is respected and the generalization level is acceptable for satellite data in an automatic context. The energy seems to be efficient since the 3D-models are correctly assembled: the obtained buildings own few artefacts and are close to the real shapes.

Figures 13, 15 and 16 show results on pieces of the Amiens downtown. The last one is a typical European downtown (i.e. an old and dense downtown with an important variety of roof types). These results are aesthetically satisfactory compared to results obtained in our previous work [16].
Figure 14 represents the energy decrease of the result obtained in Figure 13. It is the typical energy decrease (explained in the section 4.1) of a MCMC sampler using a geometric cooling schedule.

The result evaluation must be separated in two parts. We need to distinguish the ground errors (i.e. errors due to the footprint extraction stage) and the altimetric errors (i.e. the Z-errors due to the 3D-reconstruction stage). The ground errors of the proposed method have been computed in our previous work [17]. The false positive rate of footprints (in term of surface) is 9.7%. Without taking into account the low flat buildings of one floor, the true negative rate is close to 4.5%. So, the evaluation of the footprint extraction provide error rates which are correct for satellite data in an automatic context. Concerning the altimetric evaluation, it is difficult to provide error rates since we do not have accurate 3D ground truths of the reconstructed buildings and downtowns. Nevertheless, the altimetric results seem to be correct in comparaison with the IGN database.

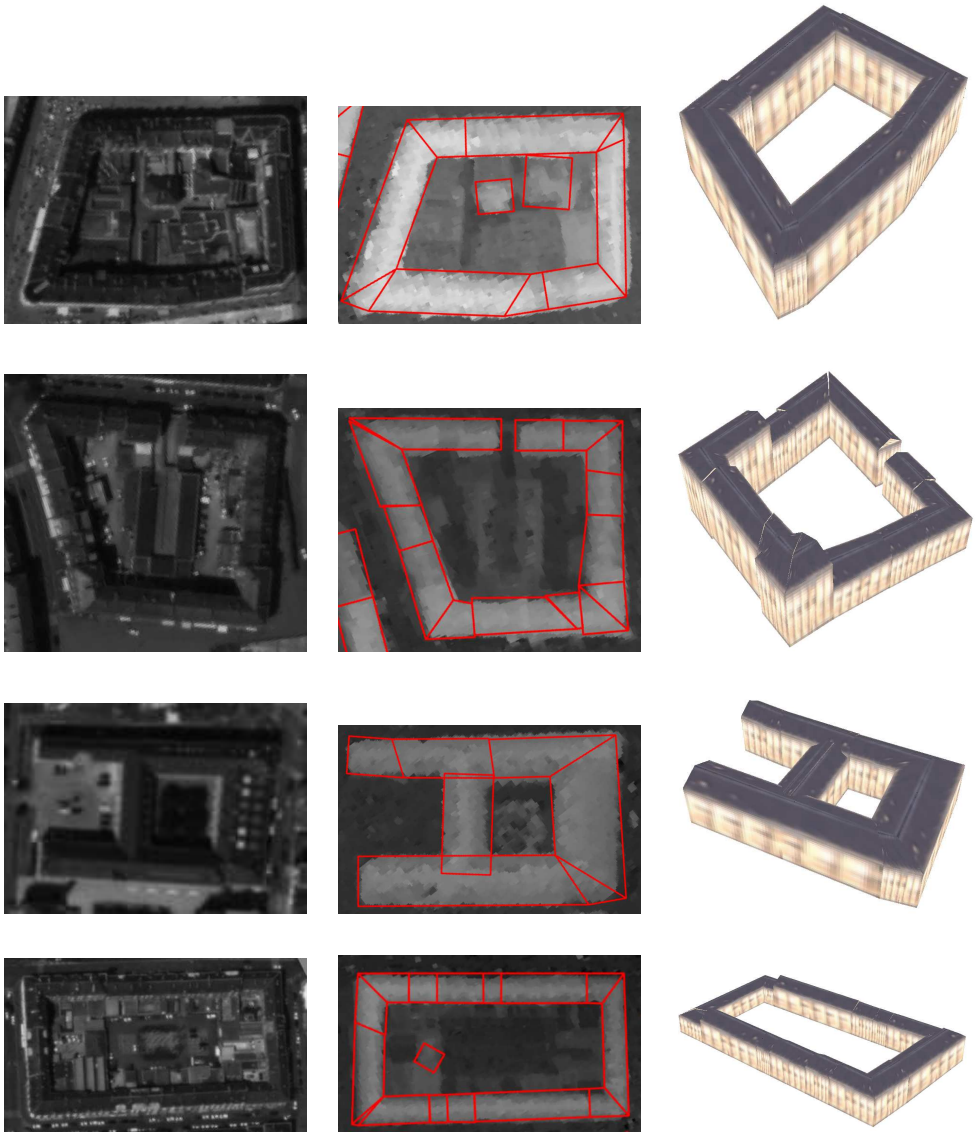

Figure 11: Examples of reconstructed buildings (right) associated with the footprint extraction results (center) and PLEIADES simulations (left)

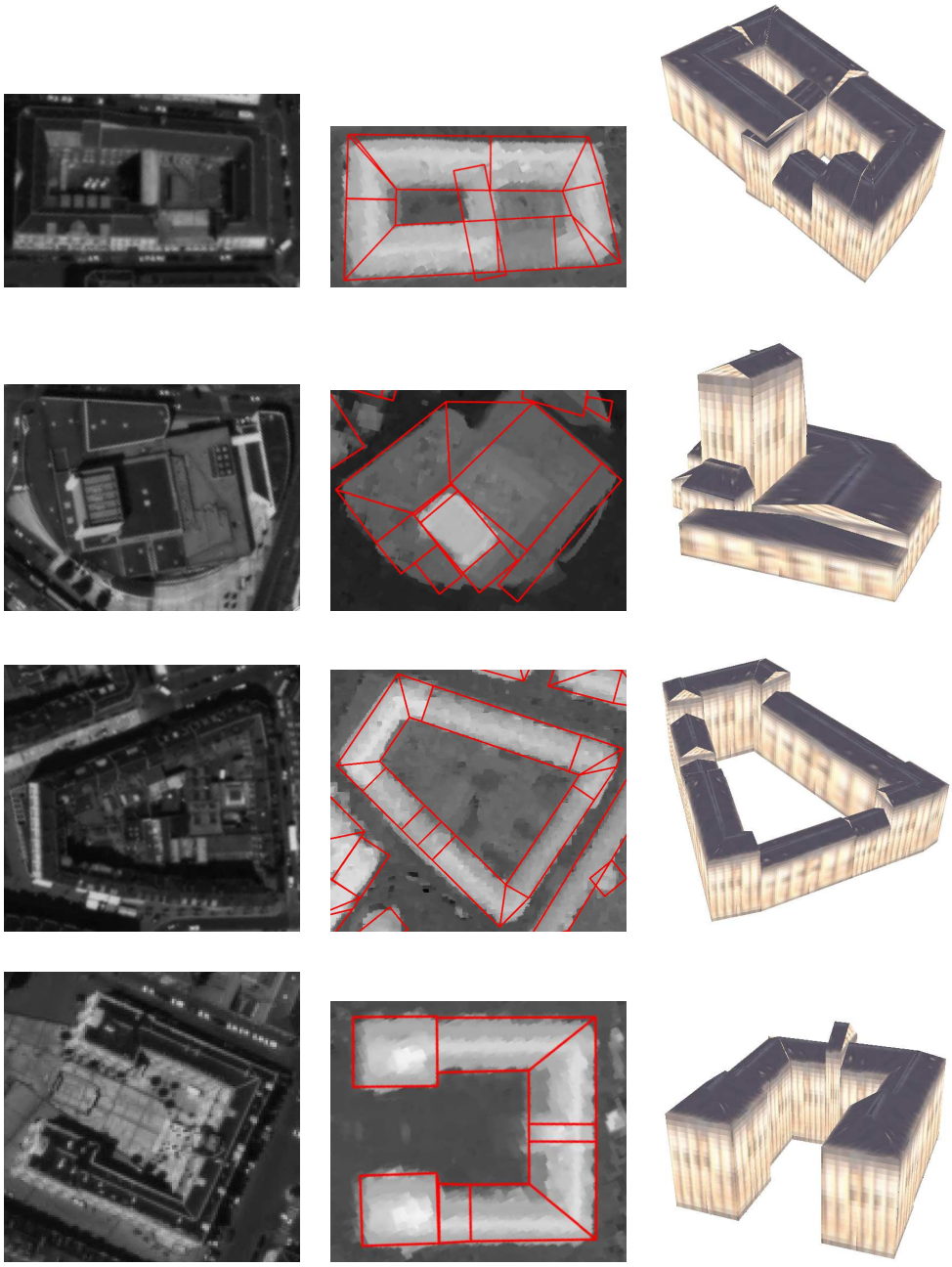

Figure 12: Examples of reconstructed buildings (right) associated with the footprint extraction results (center) and PLEIADES simulations (left)

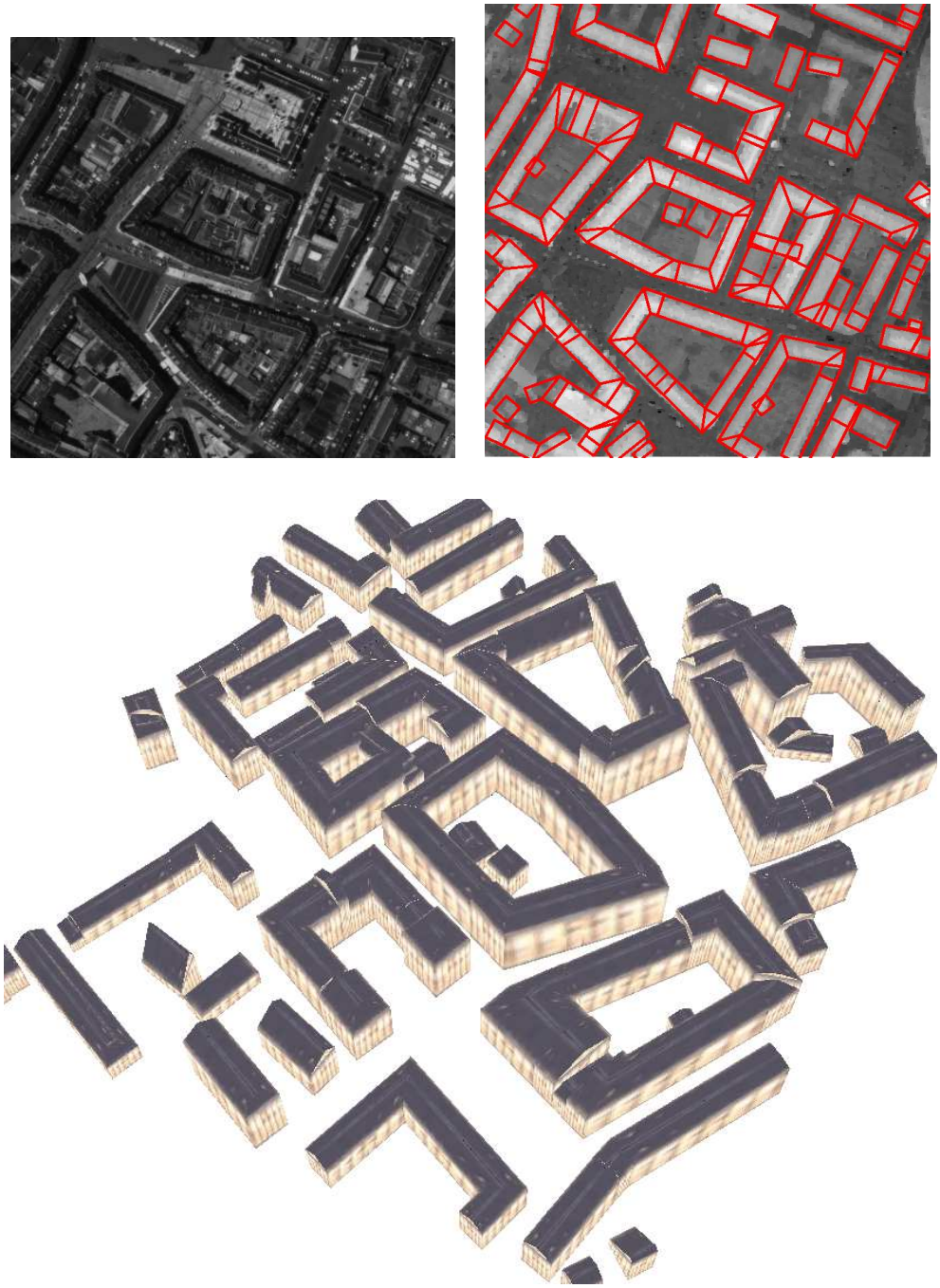

Figure 13: 3D-Result on a piece of downtown of Amiens - France related to the footprint extraction result (top right) and a PLEIADES simulation (top left)

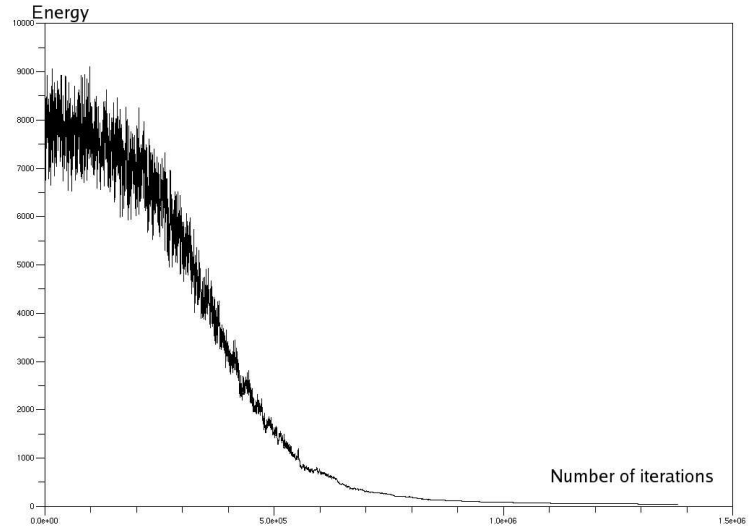

(a)

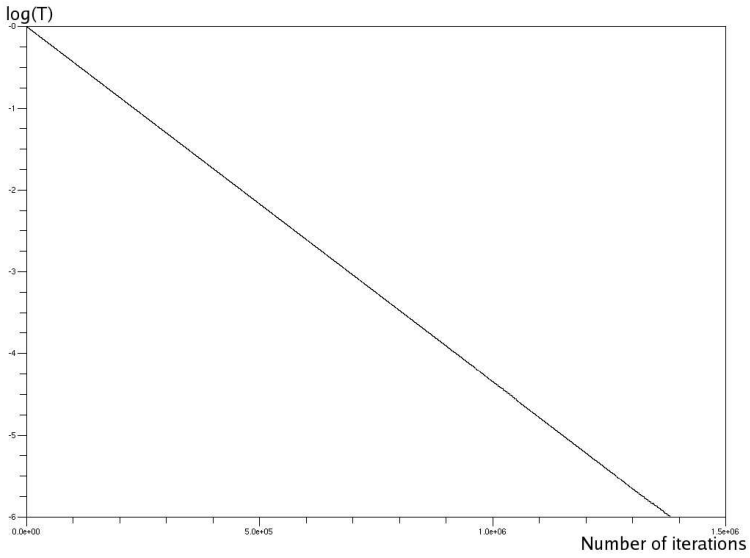

(b)

Figure 14: Energy decrease of the result obtained in Figure 13 - **(a):** energy versus the number of iterations **(b):** temperature decrease versus the number of iterations.

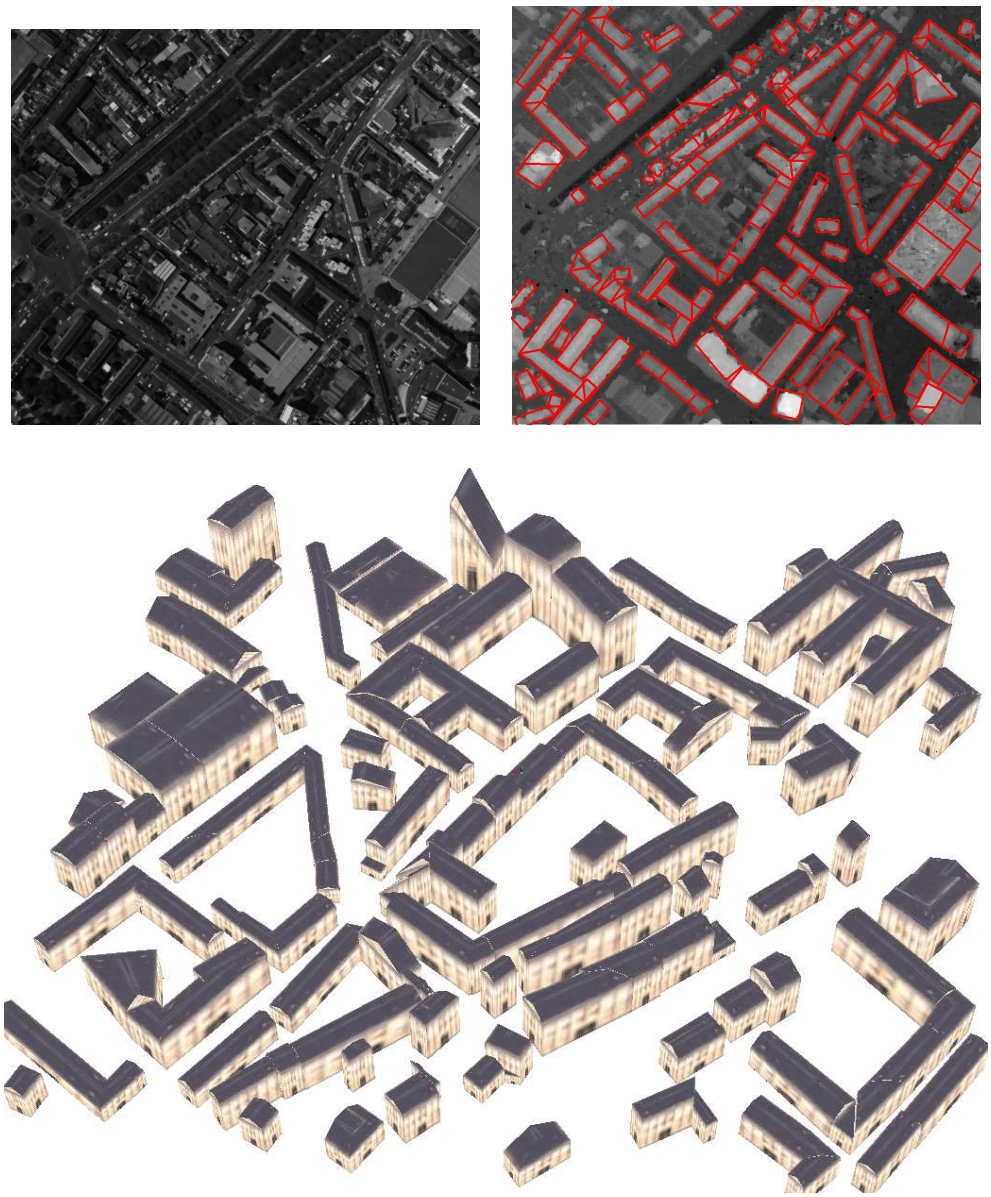

Figure 15: 3D-Result on a piece of downtown of Amiens - France related to the footprint extraction result (top right) and a PLEIADES simulation (top left)

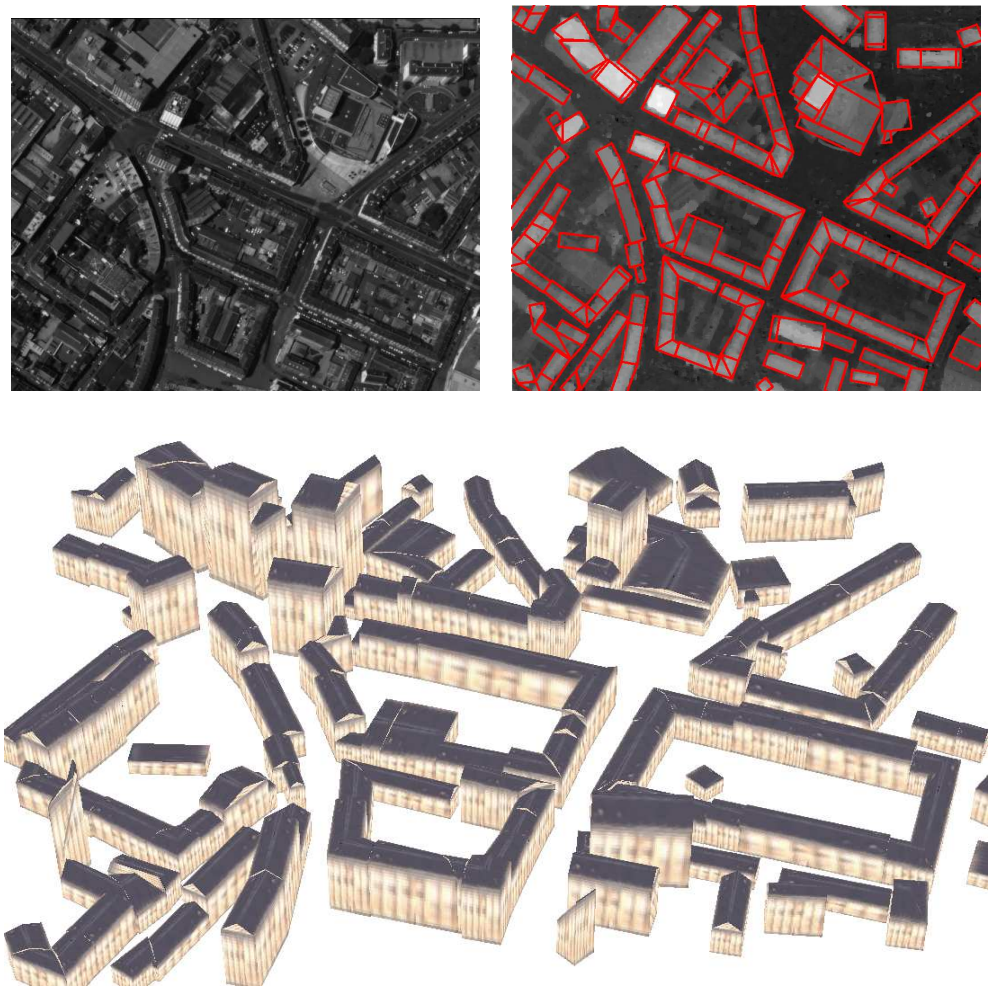

Figure 16: 3D-Result on a piece of downtown of Amiens - France related to the footprint extraction result (top right) and a PLEIADES simulation (top left)

6 Conclusion

In this report, we have proposed a 3D building reconstruction method based on a structural approach. The obtained results are good : a majority of urban structures is close to reality. This method presents several interesting characteristics:

- *the automaticity* - it is a fully automatic method which needs neither human operator interventions, nor building localization maps,
- *the robustness* - the structural approach allows to deal with low quality data by selecting relevant 3D-models with respect to the data,
- *the choice of the optimization technique* - two optimization algorithms can be used: one supports the precision w.r.t. the results, the other favors the computing time,
- *a single parameter to choose* - contrary to [16], a unique parameter must be tuned by trial and error in the Bayesian formulation,
- *an adaptive and evolutive method* - 3D-models can be added and removed in the grammar with respect to the context.

However, the good behavior of this method mainly depends on the grammar contents. It means that a priori knowledge concerning the roof types which are present in the scene are necessary to obtain good results.
In future works, it would be interesting to improve the optimization step in order to achieve both precision on the results and short computing time. One solution could be to use adaptive cooling schedules in the RJMCMC sampler. Moreover, we should evaluate the potential of this method on others kinds of cities such as typical American towns.

Acknowledgments

The first author would like to thank the French Geographic Institute (IGN) and the French Space Agency (CNES) for partial financial support during his PhD. The authors thank the French Space Agency (CNES) for providing PLEIADES simulations and Yann Bhogal from the Urban Engineering School of Paris (EIVP) for his help with the definition of the building grammar.

References

[1] C. Baillard and A. Zisserman. A plane-sweep strategy for the 3D reconstruction of buildings from multiple images. In *19th ISPRS Congress and Exhibition*, Amsterdam, The Netherlands, 2000.

[2] A.R. Dick, P.H.S. Torr, and R. Cipolla. Modelling and interpretation of architecture from several images. *International Journal of Computer Vision*, 60(2):111–134, Nov 2004.

[3] D. Flamanc and G. Maillet. Evaluation of 3D city model production from PLEIADES HR satellite images and 2D ground maps. In *URBAN*, Tempe, USA, 2005.

[4] J.D. Forney. The Viterbi algorithm. *Proceedings of the IEEE*, 13:268–278, 1973.

[5] C. Früh and A. Zakhor. Constructing 3D city models by merging aerial and ground views. *IEEE Trans. Computer Graphics and Applications*, 23(6):52–61, 2003.

[6] F. Fuchs and H. Le Men. Efficient subgraph isomorphism with a-priori knowledge. Application to building reconstruction for cartography. *Lecture Notes in Computer Science*, (1876), 2000.

[7] L. Garcin, X. Descombes, J. Zerubia, and H. Le Men. Buiding extraction using a Markov point process. In *Proc. IEEE International Conference on Image Processing (ICIP)*, Thessalonique, Grece, October 2001.

[8] P.J. Green. Reversible Jump Markov Chains Monte Carlo computation and Bayesian model determination. *Biometrika*, 57:97–109, 1995.

[9] A. Gruen and X. Wang. CC-Modeler : a topology generator for 3D city models. *ISPRS Journal of Photogrammetry and Remote Sensing*, 53(5):286–295, 1998.

[10] N. Haala and C. Brenner. Extraction of buildings and trees in urban environments. *ISPRS Journal of Photogrammetry and Remote Sensing*, 54(2-3):130–137, 1999.

[11] H. Haario and E. Saksman. Simulated annealing process in general state space. *Advances in Applied Probability*, (23):866–893, 1991.

[12] W.K. Hastings. Monte Carlo sampling using Markov chains and their applications. *Biometrica*, 57(1):97–109, 1970.

[13] H. Jibrini, M. Pierrot-Deseilligny, N. Paparoditis, and H. Maître. Automatic building reconstruction from very high resolution aerial stereopairs using cadastral ground plans. In *19th ISPRS Congress and Exhibition*, Amsterdam, The Netherlands, 2000.

[14] Z.W. Kim and R. Nevatia. Automatic description of complex buildings from multiple images. *Comput. Vis. Image Underst.*, 96(1):60–95, 2004.

[15] F. Lafarge, X. Descombes, J. Zerubia, and M. Pierrot-Deseilligny. Automatic 3D building reconstruction from DEMs: an application to PLEIADES simulations. In *Proc. of the ISPRS Commission I Symposium*, Marne La Vallee, France, July 2006.

[16] F. Lafarge, X. Descombes, J. Zerubia, and M. Pierrot-Deseilligny. An automatic building reconstruction method : A structural approach using high resolution images. In *Proc. IEEE International Conference on Image Processing (ICIP)*, Atlanta, USA, October 2006.

[17] F. Lafarge, P. Trontin, X. Descombes, J. Zerubia, and M. Pierrot-Deseilligny. An automatic building extraction method : Application to the 3D-city modeling. Research Report 5925, INRIA, France, 2006.

[18] C. Lin and R. Nevatia. Building detection and description from a single intensity image. *Comput. Vis. Image Underst.*, 72(2):101–121, 1998.

[19] H.G. Maas and G. Vosselman. Two algorithms for extracting building models from raw laser altimetry data. *ISPRS Journal of Photogrammetry and Remote Sensing*, 54(2-3):153–163, 1999.

[20] M. Metropolis, A.W. Rosenbluth, A.H. Teller, and E. Teller. Equation of state calculations by fast computing machines. *Journal of Chemical Physics*, 21:1087–1092, 1953.

[21] P. Pérez. *Modèles et algorithmes pour l'analyse probabiliste des images.* PhD thesis, University of Rennes 1, December 2003.

[22] G. Perrin, X. Descombes, and J. Zerubia. Adaptive simulated annealing for energy minimization problem in a marked point process application. In *Proc. Energy Minimization Methods in Computer Vision and Pattern Recognition (EMMCVPR)*, St Augustine, Florida, USA, November 2005.

[23] M. Pierrot-Deseilligny and N. Paparoditis. A multiresolution and optimization-based image matching approach : an application to surface reconstruction from SPOT5-HRS stereo imagery. In *Workshop ISPRS commission I*, Ankara, Turkey, 2006.

[24] L.R. Rabiner. A tutorial on hidden Markov models and selected applications in speech recognition. *Proceedings of the IEEE*, 77:257–286, 1989.

[25] C.P. Robert and G. Casella. *Monte Carlo Statistical Methods.* Springer-Verlag, New York, 1999.

[26] S. Roy and I.J. Cox. A maximum-flow formulation of the n-camera stereo correspondence problem. In *Proc. International Conference on Computer Vision (ICCV)*, Bombay, 1998.

[27] P. Salamon, P. Sibani, and R. Frost. *Facts, conjectures, and improvements for simulated annealing.* SIAM Monographs on Mathematical Modeling and Computation. Society for Industrial and Applied Mathematics, Philadelphia, 2002.

[28] S. Scholze, T. Moons, and L. Van Gool. A probabilistic approach to building roof reconstruction using semantic labelling. In *Proceedings of the 24th DAGM Symposium on Pattern Recognition*, pages 257–264, London, UK, 2002.

[29] F. Taillandier and R. Deriche. Automatic Builings Reconstruction from Aerial Images : a Generic Bayesian Framework. In *Proceedings of the XXth ISPRS Congress*, Istanbul, Turkey, 2004.

[30] P.J.M. Van Laarhoven and E.H.L. Aarts. *Simulated Annealing : Theory and Applications*. D. Reidel, Boston, 1987.

[31] J.M. Varanelli. *On the acceleration of the simulated annealing*. PhD thesis, University of Virginia, Charlottesville, U.S.A., 1996.

[32] S. Vinson and L.D. Cohen. Multiple rectangle model for buildings segmentation and 3D scene reconstruction. In *Proc. International Conference on Pattern Recognition (ICPR)*, Quebec, Canada, 2002.

[33] A.J. Viterbi. Error bounds for convolutional codes and an asymptotically optimum decoding algorithm. *IEEE Transactions on Information Theory*, 13:260–269, 1967.

[34] U. Weidner and W. Forstner. Fowards Automatic Building Reconstruction from High Resolution Digital Elevation Models. *Journal of Photogrammetry and Remote Sensing*, 50(4):38–49, 1995.

[35] S.R. White. Concepts of scale in simulated annealing. In *IEEE proc. of International Conference on Computer Design*, pages 646–651, 1984.

.

Unité de recherche INRIA Sophia Antipolis
2004, route des Lucioles - BP 93 - 06902 Sophia Antipolis Cedex (France)

Unité de recherche INRIA Futurs : Parc Club Orsay Université - ZAC des Vignes
4, rue Jacques Monod - 91893 ORSAY Cedex (France)
Unité de recherche INRIA Lorraine : LORIA, Technopôle de Nancy-Brabois - Campus scientifique
615, rue du Jardin Botanique - BP 101 - 54602 Villers-lès-Nancy Cedex (France)
Unité de recherche INRIA Rennes : IRISA, Campus universitaire de Beaulieu - 35042 Rennes Cedex (France)
Unité de recherche INRIA Rhône-Alpes : 655, avenue de l'Europe - 38334 Montbonnot Saint-Ismier (France)
Unité de recherche INRIA Rocquencourt : Domaine de Voluceau - Rocquencourt - BP 105 - 78153 Le Chesnay Cedex (France)

Éditeur
INRIA - Domaine de Voluceau - Rocquencourt, BP 105 - 78153 Le Chesnay Cedex (France)
http://www.inria.fr
ISSN 0249-6399